

PAPER • OPEN ACCESS

Image Processing Techniques for Shock Wave Detection and Tracking in High Speed Schlieren and Shadowgraph Systems

To cite this article: Guoshuai Li *et al* 2019 *J. Phys.: Conf. Ser.* **1215** 012021

View the [article online](#) for updates and enhancements.



IOP | ebooks™

Bringing you innovative digital publishing with leading voices to create your essential collection of books in STEM research.

Start exploring the [collection](#) - download the first chapter of every title for free.

Image Processing Techniques for Shock Wave Detection and Tracking in High Speed Schlieren and Shadowgraph Systems

Guoshuai Li^{1*}, Muhammed BurakAgir¹, Konstantinos Kontis¹, Takahiro Ukai²,
Sriram Rengarajan³

¹School of Engineering, University of Glasgow, Glasgow G12 8QQ, UK

²Osaka Institute of Technology, Osaka, 535-8585, Japan

³India Institute of Technology, Madras Chennai, India

g.li.1@research.gla.ac.uk

Abstract. Schlieren and shadowgraph photography has been widely used to offer insight into the flow field in aerospace engineering due to their ease of application. The high-speed schlieren and shadowgraph techniques are typically applied to investigation of unsteady shock wave structure including shock reflection patterns and shock wave/boundary layer interactions, etc. Generally, qualitative analysis is performed based on the schlieren and shadowgraph image sequences. To process and analyze the large data set of the high-speed schlieren and shadowgraph images quantitatively, especially for the shock wave detection and tracking, a software was developed based on MATLAB GUI and its image processing toolbox. In this study, the image processing techniques exploited in the software, such as background subtraction, filter, threshold, edge detection, and shock tracking are presented. A case study on the phenomena of shock wave reflection from a solid surface was conducted. The results show that the proper filter method and the background image subtraction can effectively eliminate the image noises in frequency domain, which makes it easier to analyze the flow structure. Moreover, the instantaneous locations of shock waves are detected accurately, and the shock wave propagation speed calculated using the developed software are consistent with those of previous studies.

1. Introduction

Schlieren and shadowgraph techniques have been used since the early 19th century to visualize the optical density. Most commonly, they are applicable to visualize diverse subjects such as striations in blown glass, inhalation in humans and animals, shock waves from a plane in flight, and heat emanating from a system. In the experimental fluid mechanics field, schlieren and shadowgraph techniques are widely applied to study compressible flow phenomena, such as shock waves, expansion fans, and variable-density wakes and boundary layers in the supersonic and hypersonic wind tunnels [1-12]. However, as a dynamic and straightforward visualization tool, these systems are primarily applied to conduct qualitative visual studies.

In recent years, investigations on extracting and quantifying the information from the schlieren and shadowgraph image sets using digital imaging processing and computer vision techniques have been conducted. Estruch et al. [13] employed a number of image processing algorithms such as background image subtraction and Canny edge detection methods to quantify the shock wave positions and unsteadiness. Cui et al. [14] evaluated different image edge detection algorithms including Roberts, Prewitt, Sobel Canny, and Laplacian of Gaussian for accuracy of the shock wave detection. Dehghan



et al. [15] proposed a two-level scheme involving schlieren image processing and classification to study the effects of speed change on the airplane surface.

The aim of this study is to process and quantify the large data set of the high speed schlieren and shadowgraph images more efficiently and accurately, especially for the shock wave detection and tracking. Based on improved new functions and image processing algorithms, a more versatile software system based on MATLAB GUI and its image processing toolbox was developed.

2. The proposed software system

In this section, the main functions and components of the proposed software system are described:

2.1. Basic image processing

Basic image processing functions such as image reading, saving, zooming, rotating, dragging, data cursor, image format conversion and so on are developed in the menu bar and tool bar. These functions are quite crucial and very useful for other image processing modules.

2.2. Image filter

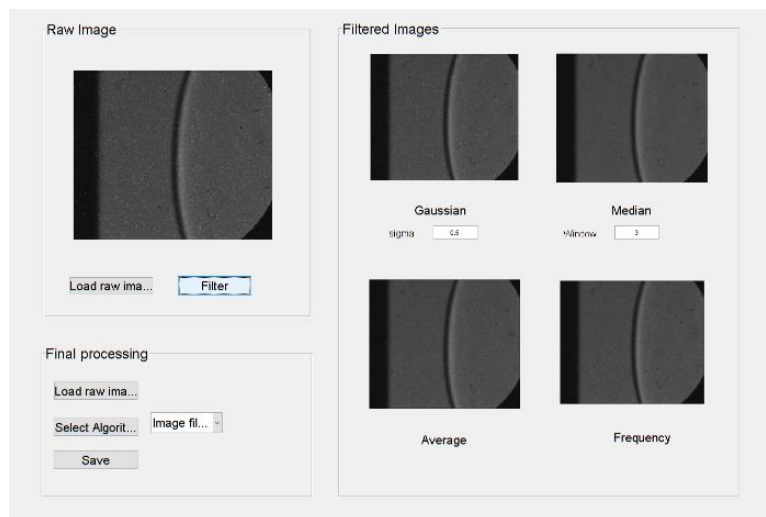


Figure 1. Image filter interface

In high speed schlieren and shadowgraph photography, the images usually contain salt-and-pepper noise and other noises due to high shutter speed and gain (ISO sensitivity). To improve the image quality and the accuracy of image threshold and shock wave detection, several image filter algorithms including Gaussian, median, average, and frequency domain filters are provided. The interface of image filtering is given in Fig. 1. Applying different filter methods and parameters, users can compare the filter effects on an image so that the optimal filter and parameters can be selected. However, it is worth noting that no algorithms can make this judgement perfectly (for all cases) since there is often a trade-off made between noise removal and preservation of fine.

2.3. Background image subtraction

The shock wave and other flow features are usually discernible as distinct dark or light regions in comparison with the background light intensity. To distinguish an image intensity more clearly and eliminate the contaminated area, an image processing routine including background image subtraction and object area restoration is applied. Fig. 2(a) shows the interface for background image subtraction processing. It is clear that the background image subtraction in the space domain and the frequency domain are both listed in the software. However, a lot of cases show that the image conversion into frequency domain using FFT can earn better results.

Unfortunately, the object area which is crucial for identifying the boundary of the flow is also deducted during the process of the background image subtraction. For restoring the object area, a threshold and restoring algorithm is proposed. The interface and the results are shown in Fig. 2 (b).

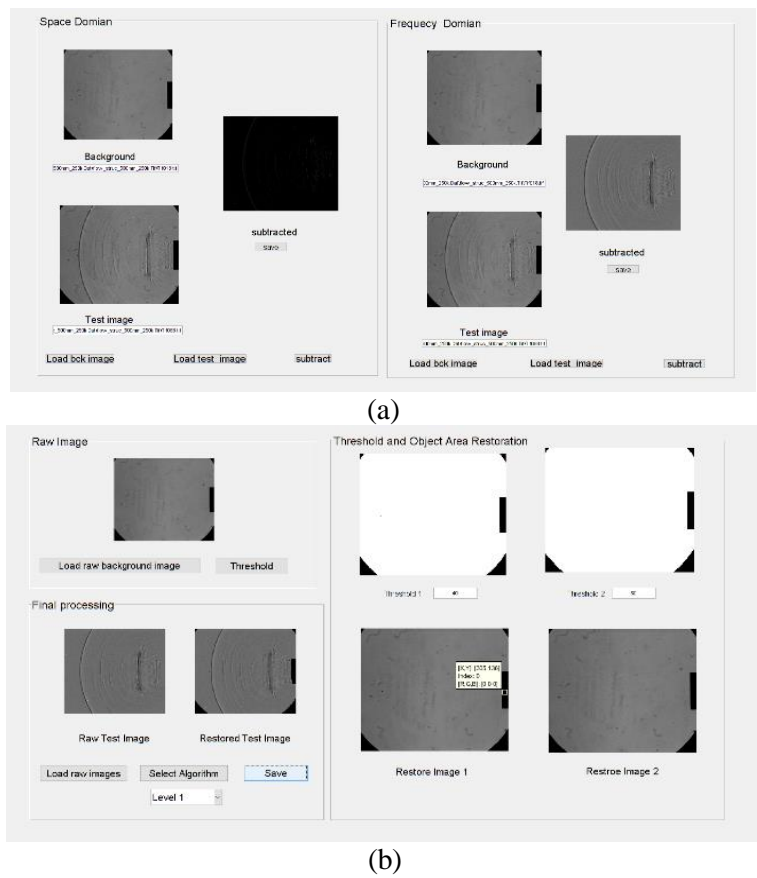
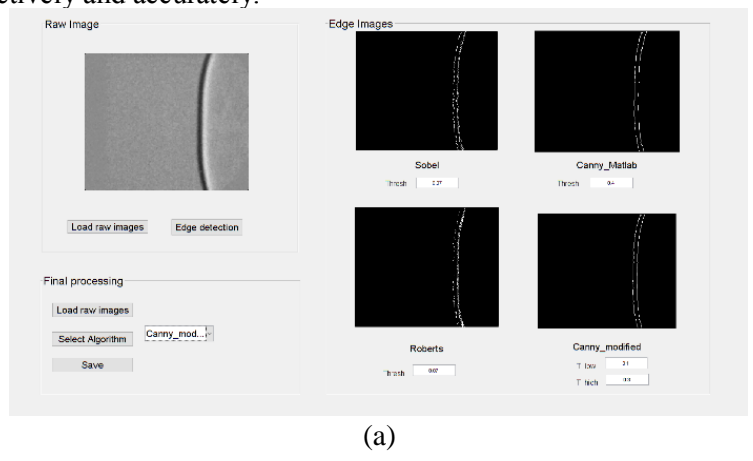


Figure 2. Background image subtraction: (a) subtracting the background image; (b) threshold and object area restoration

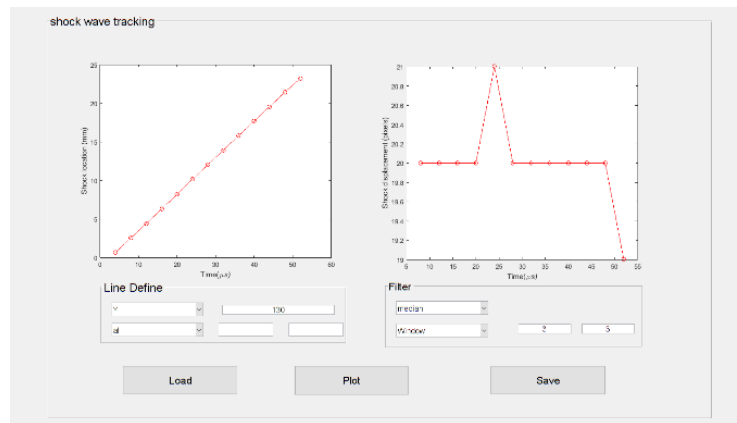
2.4. Shock wave detection and tracking

In order to detect the shape of the shock waves and other flow features, a number of edge detection algorithms are applied. The interface of edge detection in this software system is shown in Fig. 3(a). The Sobel, Canny, and Roberts edge detection algorithms have been described in the previous studies [13, 14]. To capture the steady shape unsteady change of the shock wave more accurately, a modified Canny algorithm is developed. This modified edge detection algorithm is more robust when a large amount of unsteady shock wave images need to be analyzed.

Through processing a time series of images, shock wave distortion, motion, and unsteadiness can be determined. Fig. 3 (b) shows the interface and some results of shock wave tracking. With these functions, quantitative information the schlieren and shadowgraph images contain can be extracted and quantified effectively and accurately.



(a)



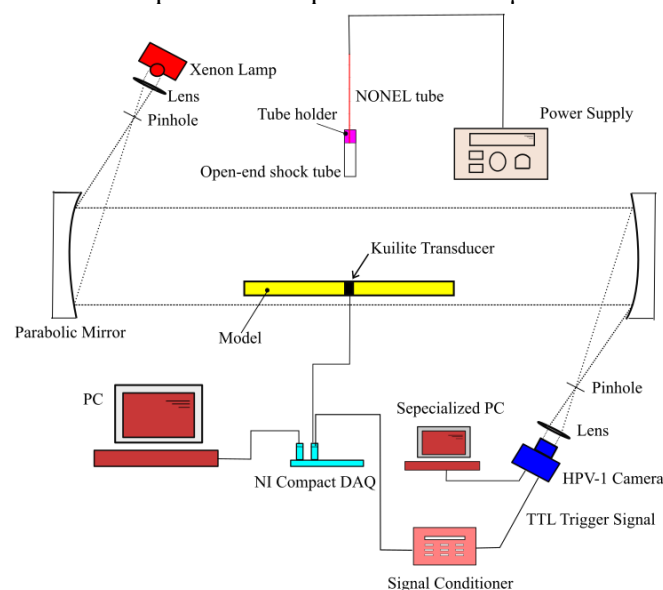
(b)

Figure 3. Shock wave detection and tracking: (a) edge detection; (b) shock wave location tracking

3. Experimental setup

The software and corresponding image processing techniques are applied in a shadowgraph visualization of the blast shock wave impingement on a solid surface. The schematic of the experimental setup is shown in Fig. 4. The open-end shock tube with the diameter $D=22\text{mm}$ consists a driven section of 200mm in length and a blasted section. A non-electric tube (Dyno Nobel, model: NONEL DynoLine) [16, 17] was used to induce a blast wave which impinges on the plate model. The detonation was initiated within the NONEL tube by an electric blasting device (Dyno Nobel, model: Dyno Start 2, output voltage: 2500 V). This explosion generates a blast wave from the NONEL tube end, and the blast wave impinged on the plate model.

Three flush-mounted pressure transducers (Kulite Semiconductor Products, Inc., model: XTE-190M, natural frequency: 175 kHz) were flush mounted along the centreline of the square plate model. The shock wave impingement and reflection process were visualised using high-speed shadowgraph photography. The shadowgraph system consists of a 450–1000W continuous light source with an Xe-Hg arc lamp (Newport, model: 66921), a pair of 203.3 mm diameter concave lens with a focal length of 1829 mm, and a high-speed camera (Shimadzu, model: HPV-1). As for the synchronization, the output of the Kulite transducer was utilized to trigger the high-speed camera. The images were acquired at a frame rate of 250 kfps with an exposure time of 1 μs .

**Figure 4.** Schematic of the experimental setup

4. Results and analysis

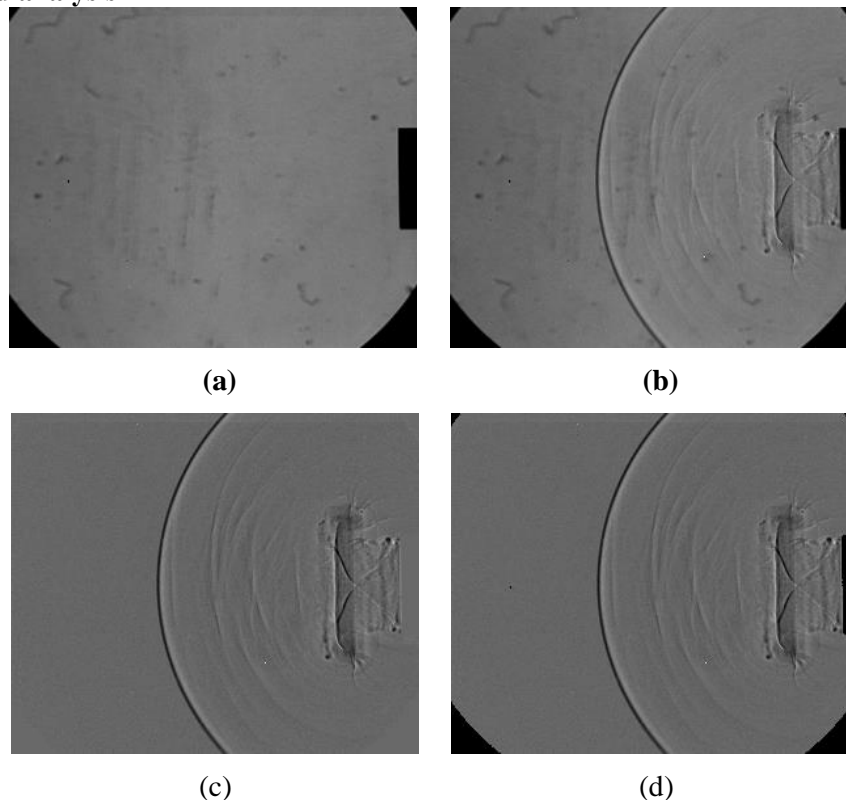


Figure 5. Background image subtraction and object area restoration of a shadowgraph image ($\Delta t = 144 \mu\text{s}$): (a) background image; (b) shadowgraph image; (c) background image subtraction; (d) object area restoration

To evaluate the visualization process and shock structure of the blast shock wave exiting from the open-end shock tube, a test case without the plate was conducted in the condition of NONEL tube of 500 mm in length. Fig. 5 shows the background image subtraction and object area restoration results of a shadowgraph image when $\Delta t = 144 \mu\text{s}$ (the elapse time after the shock wave emission from the shock tube end is defined as t_0). As shown in the Fig. 5, the original shadowgraph images have a number of image noises due to the contamination of the lens/mirror surfaces and some other reasons. This problem can be mitigated by cleaning all the optical components or improving the quality of the system hardware. In the other hand, it can be eliminated in a digital image processing viewpoint. Fig. 5 (c) shows the image processed after the background image subtraction in frequency domain. Obviously, most of the image noises are subtracted from the background image. Unfortunately, the shock tube and the regions out of measurement area in the test image are also classified as noises. The image algorithms based on threshold are developed in the software system to restore the object area. The image processing results in the subtracted shadowgraph image and object area restoration are shown in Fig. 5 (d).

The original and background image subtracted shadowgraph images are given in Fig. 6. It is apparent that subtracted shadowgraph images can distinguish the light gradient and visualize the flow structure better. In Fig. 6 (f-j), several weak shock waves behind the blast wave as well as a contact surface between the emerging and the external fluid are clearly visible. The contact surface moves away and rolls up to form a vortex ring. After the rolling up process, the vortex ring propagates and expands. In the other hand, a rearward facing shock wave with the low pressure upstream and high pressure downstream is generated. This shock wave propagates along with the vortex ring. It is worth noting that sequences of the multiple weak shock waves were observed which was also found in a previous studies [12]. Their origin is not fully understood and needs more investigations.

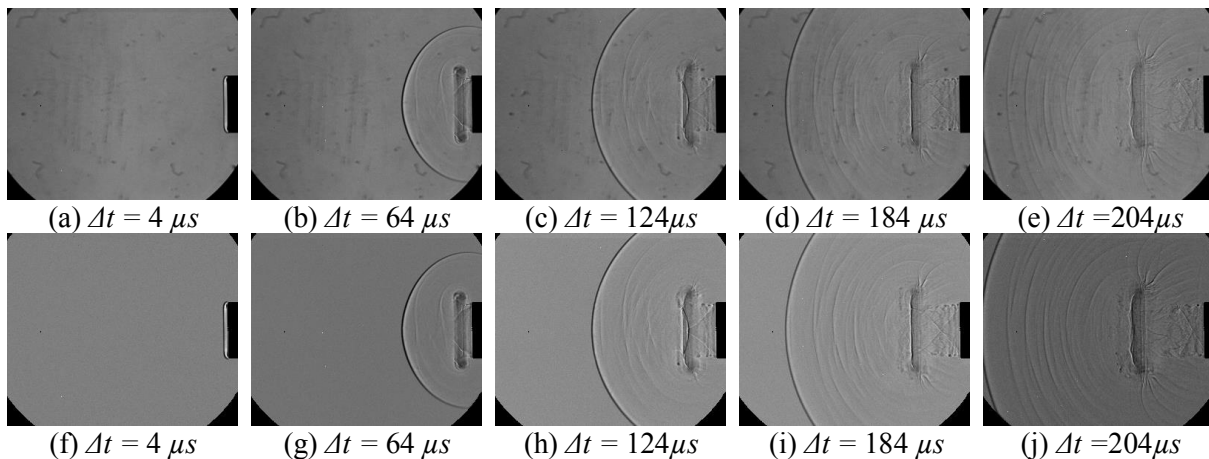
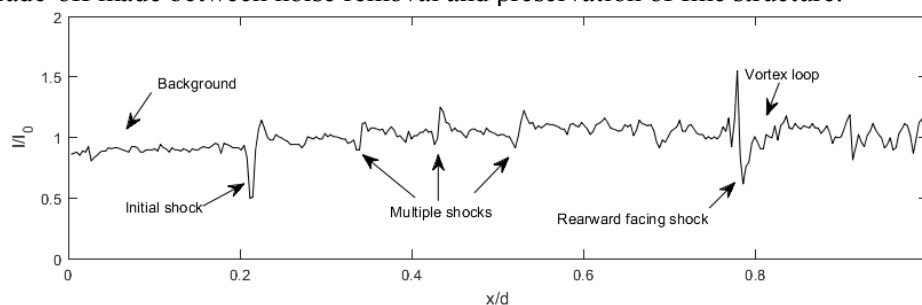


Figure 6. Time resolved shadowgraph images: (a-e) original images, (f-j) background image subtracted images

Fig. 7 gives the intensity profiles of the original and processed shadowgraph images ($\Delta t = 184 \mu s$) in their centrelines. The intensity of the density gradient was normalized by the brightness of the image background. The lateral axis denotes the normalized distance x/d from the tube end ($D = 22$ mm denotes the diameter of the shock tube). As shown in Fig. 7 (a), the locations of the blast wave, the multiple weak shock waves, the rearward facing shock wave and the vortex ring can be recognized in the intensity profile curve of the original shadowgraph image. However, there are a lot of image noises along the centreline of the shadowgraph image. Moreover, the normalized intensity varies from 0.81 to 1.01 along the background area upstream of the initial shock wave. This means that the parallel light of the shadowgraph system is not ideally uniform.

Fig. 7 (b) shows the normalized intensity profile by the background image subtraction process. The level of the noises is decreased significantly, and the locations of the flow features mentioned previously are more salient. In the meantime, the normalized intensity in the background area upstream of the initial shock wave changes from 0.962 to 1.074. The problem of the inhomogeneous incident parallel light is mitigated to some extent by background image subtraction. The normalized intensity profiles by a Gaussian filter with the standard deviation $\sigma = 0.5$ and 1.1 are shown in Fig. 7 (c) and (d), respectively. With a Gaussian filter, the random noise of the shadowgraph image is eliminated, making it easier to distinguish the main flow features such as the initial shock wave, multiple weak shock waves, rearward facing shock wave, and the vortex ring. A greater standard deviation of the Gaussian filter leads to a lower noise level, however, the boundaries of features are smoother. Namely, there is a trade-off made between noise removal and preservation of fine structure.



(a) Original shadowgraph image

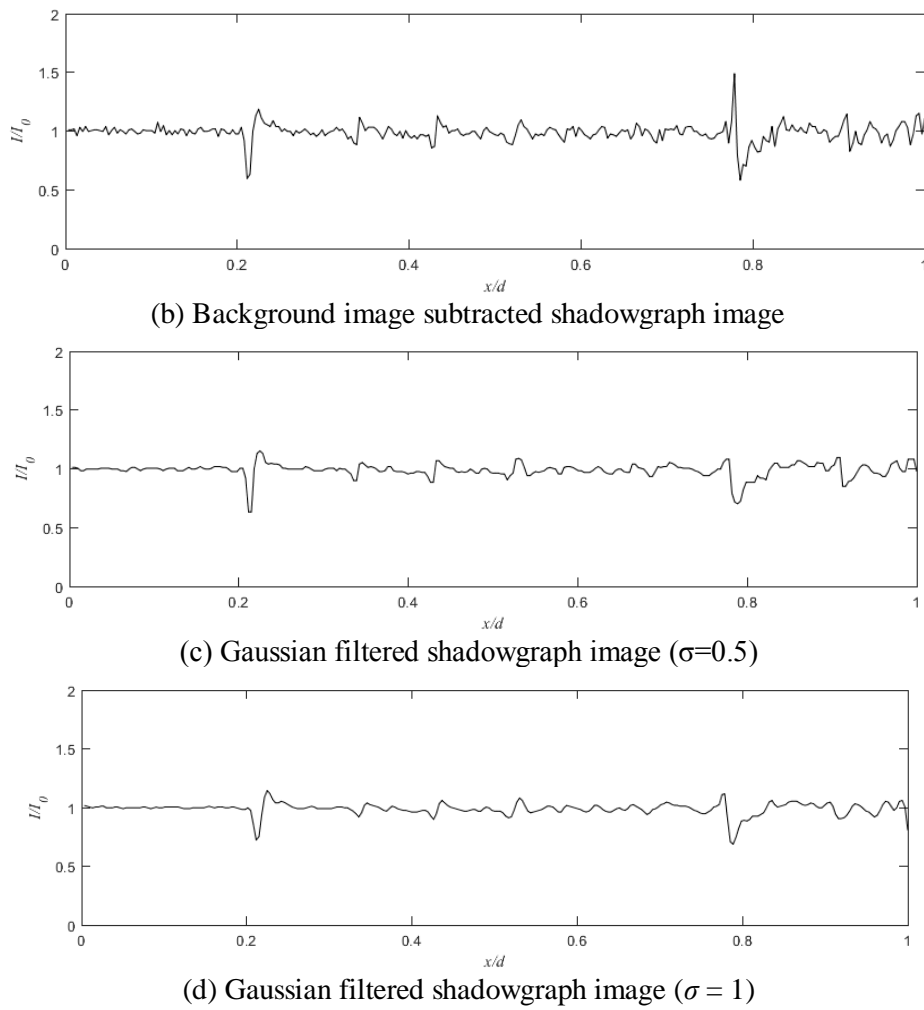


Figure 7. Intensity profiles of the original and processed shadowgraph images ($\Delta t = 184 \mu s$) in their centrelines

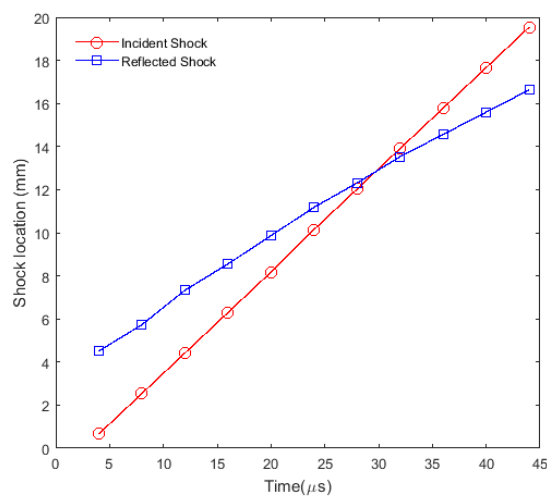


Figure 8. Instantaneous horizontal locations of the initial incident shock wave and the reflected shock wave

Furthermore, experiment regarding shock wave reflection from a solid surface was conducted based on an open-end shock tube. The distance between the tube end and the plate surface is 30 mm and the length of the NONEL tube is 300 mm. Based on a modified Canny edge detection algorithm described in the section 2, the shadowgraph images are processed to detect and track the instantaneous locations of the shock waves. The instantaneous horizontal locations of the initial incident shock and a reflected shock wave (before the reflected shock and vortex ring impingement) along the centrelines of the shadowgraph images are calculated (Fig. 8). Note that elapsed time for the incident shock is defined as t_0 when the shock wave is released from the shock tube, and the start time for the reflected shock was the time when the incident shock reaches the plate surface. Based on the shock wave movement and elapsed time, the velocity of shock wave is calculated. As shown in the Fig. 8, the velocity of the incident shock generally keeps the same and is higher than that of the reflected shock wave. The mean velocity of the incident shock wave with a 300 mm NONEL tube length is 469.8 m/s or Mach number 1.37 and the speed of the reflected shock wave is 333.5 m/s, which is a Mach number of less than 1.0. The result is very close to that of a previous study conducted by Ukai et al. [17]. Based on the shock wave detection and tracking algorithms proposed in this paper, more investigations such as shock wave movement, distortion, and unsteadiness can be performed more effectively and accurately.

5. Conclusions

A software system based on digital image processing techniques for shock wave detection and tracking in the high speed schlieren and shadowgraph techniques was developed. The primary processes includes background image subtraction, object area restoration, filter, threshold, and edge detection. To validate the image processing algorithms proposed in this paper, experiment regarding shock wave impinging on a solid surface were conducted. The result shows that image noises are eliminated effectively by background image subtraction in frequency domain and proper filter method, which makes it easier to analyse the flow structure. Moreover, the instantaneous locations of shock waves were detected accurately and the velocities of the shock waves calculated using the software were consistent with those of previous studies. Overall, the image processing techniques proposed in this paper make it more effectively to deal with the large data set of the schlieren and shadowgraph images. Investigations such as shock wave movement, distortion and unsteadiness can be conducted using the software more effectively and accurately. Next, more functions and image processing options will be extended in this software to enhance its applicability.

References

- [1] Settles, G.S. and M.J. Hargather, A review of recent developments in schlieren and shadowgraph techniques. *Measurement Science and Technology*, 2017. 28(4).
- [2] Nel, L., B. Skews, and K. Naidoo, Schlieren techniques for the visualization of an expansion fan/shock wave interaction. *Journal of Visualization*, 2014. 18(3): p. 469-479.
- [3] Daub, D., S. Willems, and A. Gülhan, Experiments on the Interaction of a Fast-Moving Shock with an Elastic Panel. *AIAA Journal*, 2016. 54(2): p. 670-678.
- [4] Desjoux, C., et al., Irregular reflection of weak acoustic shock pulses on rigid boundaries : Schlieren experiments and direct numerical simulation based on a Navier-Stokes solver. *Physics of Fluids*, 2016. 28(2).
- [5] Wolfram, J. and J. Martinez Schramm. *Pattern Recognition in High Speed Schlieren Visualization at the High Enthalpy Shock Tunnel Göttingen (HEG)*. 2010. Berlin, Heidelberg: Springer Berlin Heidelberg.
- [6] Smith, N.T., M.J. Lewis, and R. Chellappa, Detection, Localization, and Tracking of Shock Contour Salient Points in Schlieren Sequences. *AIAA Journal*, 2014. 52(6): p. 1249-1264.
- [7] Saravanan, S., et al., Schlieren Visualization of Shock Wave Phenomena over a Missile-Shaped Body at Hypersonic Mach Numbers. *Proceedings of the Institution of Mechanical Engineers, Part G: Journal of Aerospace Engineering*, 2011. 225(1): p. 26-34.
- [8] Cyril Mauger, L.M., Marc Michard, Alexandre Azouzi, Stéphane Valette, Shadowgraph, Schlieren and interferometry in a 2D cavitating channel flow. 2012.
- [9] Zare-Behtash, H., et al., Shock wave-induced vortex loops emanating from nozzles with

- singular corners. *Experiments in Fluids*, 2010. 49(5): p. 1005-1019.
- [10] Mowbray, D.E., The use of schlieren and shadowgraph techniques in the study of flow patterns in density stratified liquids. *Journal of Fluid Mechanics*, 2006. 27(03).
- [11] Clem, M.M., K. Zaman, and A.F. Fagan, Variation of shock-spacing during screech stage-jumps. *International Journal of Aeroacoustics*, 2016. 15(3): p. 324-335.
- [12] Médici, E.F. and G.P. Waite, Experimental laboratory study on the formation of multiple shock waves observed during volcanic eruptions. *Geophysical Research Letters*, 2016. 43(1): p. 85-92.
- [13] Estruch, D., et al., Measurement of shock wave unsteadiness using a high-speed schlieren system and digital image processing. *Rev Sci Instrum*, 2008. 79(12): p. 126108.
- [14] Cui, S., et al., Image Processing Techniques in Shockwave Detection and Modeling. *Journal of Signal and Information Processing*, 2013. 04(03): p. 109-113.
- [15] Dehghan Manshadi, M., et al., Speed detection in wind-Tunnels by processing schlieren images. Vol. 29. 2016. 965-970.
- [16] Samuelraj, I.O., G. Jagadeesh, and K. Kontis, Micro-blast waves using detonation transmission tubing. *Shock Waves*, 2012. 23(4): p. 307-316.
- [17] Ukai, T., et al., Three-dimensional shock wave distortion in shock-square vortex loop interaction. *Experimental Thermal and Fluid Science*, 2016. 79: p. 85-90.